bioRxiv preprint doi: https://doi.org/10.1101/2021.11.23.469707; this version posted November 23, 2021. The copyright holder for this preprint (which was not certified by peer review) is the author/funder, who has granted bioRxiv a license to display the preprint in perpetuity. It is made available under aCC-BY-NC 4.0 International license.

The RNA-binding protein Orb2 is associated with microcephaly and supports centrosome asymmetry in neural stem cells

Beverly V. Robinson[1,2], Junnan Fang[1,3], Dipen S. Mehta[3,4], Joseph Buehler[5], and Dorothy A. Lerit[1]*

Author Affiliations:

1 Department of Cell Biology, Emory University School of Medicine, Atlanta, GA 30322
2 Genetics and Molecular Biology Graduate Program, Emory University, Atlanta, GA 30322
3 These authors contributed equally
4 College of Science and Mathematics, Augusta University, Augusta, GA 30912
5 Biochemistry, Cell, and Developmental Biology Graduate Program, Emory University, Atlanta, GA 30322

* Correspondence: dlerit@emory.edu

Running title: CPEB ortholog Orb2 modulates centrosome activity

Keywords: centrosome, asymmetry, neural stem cell, Orb2, CPEB, RNA-binding protein, post-transcriptional regulation, MTOC

Funding information: This work was supported by NIH grant T32GM008490 (BVR), American Heart Association postdoctoral fellowship 20POST35210023 (to JF) and NIH grant R01GM138544 (to DAL).

bioRxiv preprint doi: https://doi.org/10.1101/2021.11.23.469707; this version posted November 23, 2021. The copyright holder for this preprint (which was not certified by peer review) is the author/funder, who has granted bioRxiv a license to display the preprint in perpetuity. It is made available under aCC-BY-NC 4.0 International license.

Abstract

To maintain a balance of self-renewal versus neurogenesis, neural stem cells (NSCs) undergo repeated cycles of asymmetric cell division along an invariant polarity axis instructed by centrosomes. During interphase, the NSC centrosomes are defined by marked asymmetries in protein composition and functional activity as microtubule-organizing centers. Here, we show a conserved RNA-binding protein, Orb2, supports centrosome asymmetry in interphase NSCs. While Orb2 localizes to the active apical centrosome, it promotes the transient inactivation of the basal centrosome required for centrosome segregation and spindle morphogenesis. Orb2 is required cell autonomously within NSCs to support centrosome asymmetry and maintenance of the stem cell pool. Conversely, loss of *orb2* manifests in microcephaly independent of Orb2 function in NSCs. We suggest Orb2 plays opposing roles in centrosome activation and inactivation, possibly through the translational regulation of multiple mRNA substrates. Bioinformatics uncovers a significant overlap among RNA targets between *Drosophila* Orb2 and human CPEB4, consistent with a conserved role for CPEB proteins in centrosome regulation and neurodevelopment.

Introduction

Neural stem cells (NSCs) undergo asymmetric cell division (ACD) along an invariant apical-basal polarity axis to segregate cell fate determinants, giving rise to two differentially fated progeny: a self-renewing stem cell and a ganglion mother cell (GMC) fated for neural differentiation (Doe et al., 1991; Knoblich et al., 1995; Kraut et al., 1996; Broadus and Doe, 1997). This balance in NSC self-renewal is critical for neurogenesis, as its deregulation can lead to brain tumors or neurodevelopmental disorders, such as microcephaly (Bond et al., 2002; Cabernard and Doe, 2009). Key to NSC homeostasis are centrosomes, which instruct the

bioRxiv preprint doi: https://doi.org/10.1101/2021.11.23.469707; this version posted November 23, 2021. The copyright holder for this preprint (which was not certified by peer review) is the author/funder, who has granted bioRxiv a license to display the preprint in perpetuity. It is made available under aCC-BY-NC 4.0 International license.

division axis and organize the bipolar mitotic spindle required to segregate the pro-stem and pro-differentiation cell fate determinants (Cabernard and Doe, 2009; Januschke and Gonzalez, 2010; Wang et al., 2011).

Centrosomes are microtubule (MT)-organizing centers (MTOC) consisting of a central pair of centrioles surrounded by pericentriolar material (PCM), which recruits the γ-Tubulin (γTub) ring complex required for MT nucleation (Conduit et al., 2015). Normally, centrosomes recruit the robust levels of PCM necessary for microtubule-nucleating activity just before mitotic onset, a process called centrosome maturation (Gould and Borisy, 1977; Khodjakov and Rieder, 1999). Following mitotic exit, centrosomes shed PCM.

In NSCs, however, centrosomes are subject to an asymmetric centrosome maturation cycle, wherein the apical (daughter) centrosome recruits PCM and organizes MTs, while the basal-fated (mother) centrosome is transiently inactivated until mitotic onset (Rebollo et al., 2007; Rusan and Peifer, 2007; Conduit and Raff, 2010; Januschke et al., 2011). NSC centrosome asymmetry is implicated in apical-basal spindle pole alignment and centrosome segregation (Januschke and Gonzalez, 2010; Januschke et al., 2013; Lerit and Rusan, 2013; Ramdas Nair et al., 2016). A basic molecular framework required for NSC centrosome asymmetry involves asymmetric localization of Centrobin (Cnb) and Polo kinase to the daughter centrosome in a mechanism also requiring Wdr62 to promote centrosome maturation (Januschke et al., 2013; Ramdas Nair et al., 2016; Gallaud et al., 2020). Conversely, transient inactivation of the basal centrosome requires Bld10/Cep135, Pericentrin-like protein (PLP), and Polo-like kinase 4 (PLK4/SAK) (Lerit and Rusan, 2013; Singh et al., 2014; Gambarotto et al., 2019). Nevertheless, how centrosome asymmetry is regulated remains incompletely understood.

Intriguingly, *Cnb*, *Cep135*, *plp*, *polo*, and *Wdr62* mRNAs were identified as putative mRNA targets for the RNA-binding protein (RBP) Orb2 through an unbiased transcriptomics

bioRxiv preprint doi: https://doi.org/10.1101/2021.11.23.469707; this version posted November 23, 2021. The copyright holder for this preprint (which was not certified by peer review) is the author/funder, who has granted bioRxiv a license to display the preprint in perpetuity. It is made available under aCC-BY-NC 4.0 International license.

study, raising the possibility that Orb2 might regulate centrosome asymmetry in NSCs (Stepien et al., 2016). Orb2 is a member of the cytoplasmic polyadenylation element binding (CPEB) proteins orthologous to mammalian CPEB2–4 and implicated in mRNA localization and translational control (Huang et al., 2006; Keleman et al., 2007; Hafer et al., 2011). Although prior work supports a role for *orb2* in NSC spindle orientation and neuronal specification, whether Orb2 contributes to centrosome regulation is unknown (Hafer et al., 2011).

Here, we identify an NSC-autonomous role for Orb2 in establishing centrosome asymmetry associated with misaligned spindles and NSC loss. We also identify an NSC-independent role for Orb2 in regulating brain size, as *orb2* loss leads to microcephaly. Finally, we examine potential targets of Orb2 and propose a revised model of asymmetric centrosome maturation.

Results and Discussion

Orb2 disrupts centrosome activity in interphase NSCs

To determine if Orb2 contributes to centrosome asymmetry, we examined γTub distributions at apical and basal centrosomes in wild-type (WT) vs. *orb2* null mutant NSCs during late interphase, when centrosomes are normally asymmetric (Rebollo et al., 2007; Rusan and Peifer, 2007). To directionally measure protein localization to centrosomes, we calculated an asymmetry index (AI; *Methods*), wherein a value near 0 indicates symmetric distribution, while values near 1 or -1 indicate asymmetric enrichment at the apical or basal centrosome, respectively. Centrosomes visualized with the centriole marker Asterless (Asl; (Varmark et al., 2007) displayed the expected symmetric distribution among apical and basal centrosomes in both genotypes (mean AI $\pm$ S.D.= 0.0$\pm$0.2 for WT and 0.1$\pm$0.3 for *orb2*; Fig. 1A–C). In comparison, γTub was significantly enriched on the apical centrosome in WT NSCs (Fig. 1A, C).

bioRxiv preprint doi: https://doi.org/10.1101/2021.11.23.469707; this version posted November 23, 2021. The copyright holder for this preprint (which was not certified by peer review) is the author/funder, who has granted bioRxiv a license to display the preprint in perpetuity. It is made available under aCC-BY-NC 4.0 International license.

In contrast to WT, *orb2* NSCs showed impaired centrosome asymmetry, evident by increased γTub localization to the basal centrosome and decreased AI values (Fig. 1B, C). γTub AI was reduced by over 20% within *orb2* NSCs, as compared to WT (Fig 1C; p=0.05 by Kolmogorov-Smirnov test). Consistently, ~30% of *orb2* NSCs (N= 12/40) had γTub AI values >2 S.D. from the WT mean (Fig 1D; p< 0.0001 by chi-square test). Measuring the levels of γTub localized at the apical and basal centrosomes revealed a 2.7-fold increase in γTub recruitment to the basal centrosomes of symmetrized *orb2* NSCs relative to WT (Fig. 1E; p<0.0001 by Mann-Whitney test). We conclude Orb2 primarily promotes centrosome asymmetry during interphase by blocking the precocious activation of the basal centrosome, although diminished recruitment of γTub to the apical centrosome may compound this effect.

Orb2-dependent centrosome regulation is cell autonomous

ACD is regulated through intrinsic and extrinsic cellular pathways (Siegrist and Doe, 2006; Doe, 2008). Prior work indicates Orb2 is broadly expressed throughout the larval central nervous system (Keleman et al., 2007; Hafer et al., 2011). To elucidate if the reduction of centrosome asymmetry observed in *orb2* mutants arose from a requirement for Orb2 within NSCs, we depleted *orb2* specifically in NSCs using an *orb2* dsRNA transgene (*UAS-orb2*^{RNAi}) driven by the NSC-specific *worniu* (*wor*)-*GAL4* (Albertson et al., 2004). Both the no *GAL4* control and the *wor-GAL4>orb2*^{RNAi} (hereafter, *orb2*^{RNAi}) interphase NSCs showed equal distributions of Asl at apical and basal centrosomes (Fig. 1F–H). While controls appeared WT with an enrichment of γTub on the apical centrosome, a subset of *orb2*^{RNAi} NSCs (~30%; N=16/51) recruited γTub to the basal centrosome precociously and showed reduced γTub at the apical centrosome (Fig. 1G–J). These data indicate Orb2 promotes centrosome asymmetry cell autonomously within NSCs through opposing activities at the apical and basal centrosomes.

bioRxiv preprint doi: https://doi.org/10.1101/2021.11.23.469707; this version posted November 23, 2021. The copyright holder for this preprint (which was not certified by peer review) is the author/funder, who has granted bioRxiv a license to display the preprint in perpetuity. It is made available under aCC-BY-NC 4.0 International license.

Loss of *orb2* is associated with supernumerary centrosomes

The precocious activation of the basal centrosome is associated with errant centrosome segregation during ACD, resulting in both centrosomes retained within the self-renewing stem cell (Lerit and Rusan, 2013). To assay whether *orb2* loss similarly impairs centrosome segregation, we quantified the frequency of supernumerary centrosomes in WT and *orb2* NSCs. While >90% WT NSCs (N=25/30) had the expected 2 centrosomes, ~35% *orb2* mutant NSCs (N=15/40) had extra centrosomes (Fig 2A–C; $p<0.05$ by chi-square test). A similar frequency of supernumerary centrosomes was observed in $orb2^{RNAi}$ NSCs (~25%; N=13/51; $p<0.05$ by chi-square test), demonstrating Orb2 functions within NSC to regulate centrosome number, likely due to failed segregation of the basal centrosome to the GMC (Fig. 2D–F).

Orb2 is required for mitotic spindle morphogenesis

Given that Orb2 helps regulate centrosome activity and segregation, we next examined its role in spindle orientation. During ACD, the NSC mitotic spindle normally orients along an invariant apical-basal polarity axis entrained by the concerted action of multiple protein complexes (Siegrist and Doe, 2005; Siller et al., 2006; Cabernard and Doe, 2009). Apical polarization is initiated by the Par-complex, comprising Bazooka (Baz)/Par-3, Par-6, and atypical protein kinase C (αPKC; (Kuchinke et al., 1998; Cai et al., 2003; Goldstein and Macara, 2007)). Inhibitory phosphorylation events by αPKC restrict basal fate determinants and the adapter protein Miranda (Mira) to the basal cortex (Betschinger et al., 2003; Atwood and Prehoda, 2009).

We examined polarity establishment in mitotic WT and *orb2* NSCs by monitoring the localization of Baz and Mira. Localization of Baz to the apical cortex in late interphase initiates NSC polarization (Wodarz and Huttner, 2003; Knoblich, 2008), while localization of Mira to the basal cortex during mitosis represents a late polarization step (Shen et al., 1998; Rolls et al.,

bioRxiv preprint doi: https://doi.org/10.1101/2021.11.23.469707; this version posted November 23, 2021. The copyright holder for this preprint (which was not certified by peer review) is the author/funder, who has granted bioRxiv a license to display the preprint in perpetuity. It is made available under aCC-BY-NC 4.0 International license.

2003; Atwood and Prehoda, 2009). WT and *orb2* mutant NSCs showed similar distributions of Baz and Mira to the apical and basal cortices, respectively (Fig 2G–I; n.s. by chi-square test). These data argue that polarization is not significantly disrupted in *orb2* larval NSCs.

We next used multiple coordinate analysis to define spindle orientation in WT and *orb2* NSCs stained for β-Tubulin to label MTs, Baz, and Asl (see *Methods*; Fig. 2J–L). First, we measured spindle orientation (θ_1),, the angle between the apical cortical polarity and spindle alignment axes (Fig. 2J, M–N). In WT, most spindles aligned within 30° of the polarity axis, yet ~20% of *orb2* NSC spindles were misoriented >30°, indicating *orb2* spindles are more randomized than controls (Fig 2M, N; $p<0.0001$ by chi-square test).

To ascertain how defects in spindle orientation arise, we next quantified apical polarity alignment, θ_2, the angle between the apical centrosome and polarity axes (Fig. 2J, O–P). The anchoring of the apical centrosome to the apical cortex happens during early interphase and influences polarization in NSCs and other stem cells (Yu et al., 2003; Januschke and Gonzalez, 2010; Inaba et al., 2015). Both WT and *orb2* NSCs showed alignment of the apical centrosome to the apical polarity axis, consistent with our observations that apical polarity is unaffected in *orb2* mutants (Fig. 2G-I, O-P).

Finally, we examined centrosome alignment, θ_3, the angle between the apical and basal centrosome axes (Fig 2J, Q-R). About 90% of WT mitotic NSCs aligned the basal centrosome ~180° away from the apical centrosome (Fig 2K, Q-R). In contrast, θ_3 is reduced in *orb2* NSCs (Fig. 2L, Q). While the average reduction in θ_3 is not statistically significant, a subpopulation of *orb2* NSCs (~20%; N=7/32 cells) show defective θ_3 <120° (Fig. 2L, Q). Consequently, spindle morphogenesis is significantly impaired, resulting in a higher frequency (~25%; N=9/34 cells; $p<0.0001$ by chi-square test) of bent spindles in *orb2* NSCs relative to WT (Fig 2R). Taken together, these data argue the precocious activation of the basal centrosome in *orb2* NSCs during interphase impairs centrosome migration to the basal cortex, resulting in aberrant spindle

bioRxiv preprint doi: https://doi.org/10.1101/2021.11.23.469707; this version posted November 23, 2021. The copyright holder for this preprint (which was not certified by peer review) is the author/funder, who has granted bioRxiv a license to display the preprint in perpetuity. It is made available under aCC-BY-NC 4.0 International license.

alignment and morphology. Alternatively, *orb2* may have a distinct functions in interphase centrosome asymmetry and mitotic spindle orientation.

Loss of *orb2* results in microcephaly

Defects in centrosome regulation contribute to neurodevelopmental disorders, including microcephaly and intellectual disability (Robinson et al., 2020). Previous work illustrates *orb2* is crucial for learning and memory in the adult *Drosophila* brain (Keleman et al., 2007; Mastushita-Sakai et al., 2010; Kruttner et al., 2012; Kacsoh et al., 2015; Hervas et al., 2016; Sanguanini and Cattaneo, 2018). Moreover, reduced brain volumes were noted from serial sectioning adult *orb2* brains (Kruttner et al., 2012). Thus, to assess larval neurodevelopment in *orb2* mutants, we measured the volume of single optic lobes from age-matched third instar larva (Link et al., 2019). Compared to WT brains, *orb2* brains were significantly smaller (Fig 3A,B,E; $p<0.0001$ by t-test). About 75% (N=10/13 cells) of *orb2* brains had volumes < 2-S.D. from WT, consistent with microcephaly.

To determine if NSC loss contributes to *orb2*-dependent microcephaly, we counted the number of Mira+ NSCs in control and *orb2* brains. While WT had ~80 NSCs, *orb2* mutants showed a ~20% reduction with ~60 NSCs per lobe (Fig 3C,D,F; $p<0.001$ by t-test). These data indicate Orb2 is required to maintain the NSC pool.

Are the centrosome and spindle defects observed in *orb2* mutants correlated with NSC loss and/or microcephaly? To begin to address this question, we depleted *orb2* specifically in NSCs and compared the brain volume of age matched $orb2^{RNAi}$ brains relative to no *GAL4* controls and noted no difference (Fig. 3 G,H,K), indicating *orb2*-dependent microcephaly is nonautonomous to NSCs – Orb2 is required in other cell types to affect brain size. In contrast, NSC loss is a cell autonomous response to *orb2* depletion. Similar to *orb2* mutants, we detected ~30% fewer NSC per optic lobe in $orb2^{RNAi}$ brains relative to no *GAL4* controls (Fig 3I,J,L; $p<0.0001$ by t-test). We conclude the frequency of NSC loss in *orb2* mutants is similar to the

bioRxiv preprint doi: https://doi.org/10.1101/2021.11.23.469707; this version posted November 23, 2021. The copyright holder for this preprint (which was not certified by peer review) is the author/funder, who has granted bioRxiv a license to display the preprint in perpetuity. It is made available under aCC-BY-NC 4.0 International license.

incidence of centrosome defects, arguing these responses are correlated. Moreover, NSC loss may be uncoupled from *orb2*-dependent microcephaly, consistent with the idea that Orb2 supports neurodevelopment in multiple cellular lineages.

To elucidate mechanisms underlying NSC loss in *orb2* mutants, we first tested the hypothesis that NSCs are eliminated by cell death. We quantified the coincidence of pro-apoptotic cleaved Caspase 3 (CC3; (Fan and Bergmann, 2010)) in cells marked with the NSC-specific Deadpan (Dpn) antibody (Bier et al., 1992). Similar rates of apoptosis were observed in WT and *orb2* NSCs, indicating NSC loss occurs by other mechanisms (Fig S1 A–C; n.s. by t-test). Another mechanism whereby NSCs may be depleted is via premature differentiation (Cabernard and Doe, 2009; Lai and Doe, 2014; Abdel-Salam et al., 2020). Normally, the pro-differentiation marker Prospero (Pros) is confined to the nucleus of the differentiating GMCs and absent from NSCs (Doe et al., 1991; Vaessin et al., 1991), while retention of Pros in the NSC nucleus promotes premature differentiation (Lai and Doe, 2014). We quantified the coincidence of Pros with Dpn and detected no significant difference relative to WT, indicating premature differentiation does not precipitate NSC loss in *orb2* mutants (Fig S1D–F; n.s. by t-test).

Finally, we examined whether *orb2* affects mitotic progression, reasoning impaired NSC self-renewal might contribute to NSC loss. However, the mitotic indices in WT and *orb2* brains were not significantly different (33.6$\pm$4.9% per lobe in N=6 WT vs. 36.3$\pm$10.1% in N=10 *orb2* brains; Fig S1G–I; n.s. by t-test). These data suggest NSC loss is not due to increased quiescence. Loss of NSCs observed in *orb2* mutants may be actuated by non-apoptotic cell death pathways. Alternatively, the altered neuronal specification observed in *orb2* embryos may impinge upon larval neurodevelopment, resulting in fewer NSCs (Hafer et al., 2011).

Orb2 localizes to centrosomes within cycling NSCs

Our data indicate Orb2 functions autonomously within NSCs to regulate centrosome asymmetry. Previous work indicates CPEB proteins localize to centrosomes in *Xenopus*

bioRxiv preprint doi: https://doi.org/10.1101/2021.11.23.469707; this version posted November 23, 2021. The copyright holder for this preprint (which was not certified by peer review) is the author/funder, who has granted bioRxiv a license to display the preprint in perpetuity. It is made available under aCC-BY-NC 4.0 International license.

240 embryos and cultured mammalian cells (Groisman et al., 2000; Pascual et al., 2020a; Pascual
241 et al., 2020b). Although Orb2 localizes to neuronal lineages, subcellular localization of Orb2 is
242 not well defined (Keleman et al., 2007; Hafer et al., 2011). Therefore, to inform mechanisms of
243 how Orb2 functions within NSCs to support centrosome asymmetry and spindle morphogenesis,
244 we examined endogenous Orb2 localization in NSCs using monoclonal antibodies (Hafer et al.,
245 2011). In interphase NSCs, Orb2 appeared dispersed throughout the cytoplasm with a notable
246 enrichment on the apical centrosome (Fig 4A, *interphase*). Apical centrosome enrichment of
247 Orb2 was observed in N=21/24 interphase NSCs, indicated by positive Orb2 AI values (Fig. 4B).
248 On average, interphase apical centrosomes contained 1.7-fold more Orb2 than basal
249 centrosomes (Fig. 4C; $p<0.01$ by t-test). Upon mitotic entry, Orb2 localization increased at both
250 centrosomes, demonstrating Orb2 is recruited to active centrosomes during centrosome
251 maturation (Fig 4A, *prophase* and *metaphase*). Our localization analysis reveals two populations
252 of Orb2 in interphase NSCs, a cytoplasmic versus centrosomal pool, raising the possibility that
253 Orb2 may normally function to regulate centrosome activity locally at centrosomes, from a
254 distance within the cytoplasm, or both.
255
256
257 **Orb2 regulates PLP protein levels in larval brains**
258 Because Orb2 is an RNA-binding protein known to promote or repress translation of its target
259 mRNAs, we reasoned it may contribute to centrosome regulation indirectly through regulation of
260 an mRNA associated with centrosome asymmetry (Mastushita-Sakai et al., 2010; Xu et al.,
261 2012; Khan et al., 2015). A genome-wide analysis for mRNA targets bound by Orb2 within
262 *Drosophila* S2 cell extracts uncovered thousands of putative targets, including mRNAs of genes
263 required for NSC centrosome asymmetry, e.g., *Cep135*, *Cnb*, *plp*, *polo*, and *Wdr62* mRNAs
264 (Januschke et al., 2013; Lerit and Rusan, 2013; Singh et al., 2014; Ramdas Nair et al., 2016;
265 Stepien et al., 2016; Gallaud et al., 2020). While these transcripts were identified as potential

bioRxiv preprint doi: https://doi.org/10.1101/2021.11.23.469707; this version posted November 23, 2021. The copyright holder for this preprint (which was not certified by peer review) is the author/funder, who has granted bioRxiv a license to display the preprint in perpetuity. It is made available under aCC-BY-NC 4.0 International license.

Orb2 targets, they varied in their biologic complexity (BC), a metric of reproducibility across biological replicates (Licatalosi et al., 2008).

Aspects of the *orb2* null phenotype in NSCs resemble *plp* loss, as both mutants display precocious activation of the basal centrosome in interphase NSCs coincident with supernumerary centrosome and spindle defects (Lerit and Rusan, 2013). Given these similarities, we tested if Orb2 regulates PLP protein expression by comparing PLP levels in WT vs. *orb2* larval brain extracts. Semi-quantitative western blotting uncovered an average 30% reduction in PLP in *orb2* relative to WT, suggesting Orb2 promotes PLP translation (Fig. 5A, B). To assay a requirement for Orb2 in regulating PLP in NSCs, we examined PLP localization to the apical versus basal centrosomes in interphase NSCs. In WT NSCs, PLP was enriched on the inactive, basal centrosome, consistent with prior work (Fig. 5C; (Lerit and Rusan, 2013; Singh et al., 2014). Despite a reduction in PLP levels in whole brain extracts, robust localization of PLP to centrosomes was detected in *orb2* NSCs, comparable to WT (Fig. 5C, D; n.s. by Kolmogorov-Smirnov test). Further, levels of PLP localized at apical vs. basal centrosomes were not significantly different from WT (Fig. 5E). Taken together, these data imply Orb2-dependent regulation of PLP may occur outside of NSCs and raise the possibility that other Orb2 targets contribute to NSC centrosome regulation.

To refine the list of targets that may be involved in NSC centrosome regulation, we compared the Orb2 mRNA targets identified in *Drosophila* S2 cells (Stepien et al., 2016) to a recent list of mRNA targets bound by CPEB4 in HeLa cells (Pascual et al., 2020b) and identified 1083 overlapping genes (Fig S2A; Table S1). Gene ontology (GO) analysis for cellular components uncovered a significant enrichment of organelle terms (Fig S2B). In contrast, centrosome-related ontologies were not significantly enriched among the overlapping genes (Fig S2C). However, because Orb2 has multiple orthologs, CPEB2-4, other putative Orb2 targets absent from the CPEB4 dataset are omitted from these pairwise analyses. Therefore, we examined centrosome-related ontologies of Orb2 targets with a BC $\geq$ 3. This analysis

bioRxiv preprint doi: https://doi.org/10.1101/2021.11.23.469707; this version posted November 23, 2021. The copyright holder for this preprint (which was not certified by peer review) is the author/funder, who has granted bioRxiv a license to display the preprint in perpetuity. It is made available under aCC-BY-NC 4.0 International license.

identified 2150 mRNAs, among which 53 mRNAs were annotated with centrosome ontologies, which may be subject to Orb2 regulation (Fig. S2D; Table S1).

Model Summary

Our data indicate Orb2 is required for robust inactivation of the basal centrosome and may also enhance apical centrosome activity in interphase NSCs. Orb2 also functions in other cell types for normal brain size (Fig 5F). Given its local enrichment, we propose Orb2 promotes apical centrosome maturation (Fig 5F, *top box*), while cytoplasmic Orb2 inactivates the basal centrosome, perhaps by repressing pro-maturation factors (Fig 5F, *bottom box*). Consistent with opposing activities at the apical vs. basal centrosomes, Orb2 activates or represses the translation of its targets depending on its oligomerization status ((Khan et al., 2015)). This model predicts cytoplasmic Orb2 is predominantly monomeric, thereby functioning as a translational repressor, while centrosome-localized Orb2 is oligomerized and functions as a translational activator. Whether on-site translation occurs at the apical centrosome remains to be tested and specific Orb2 targets require identification.

Microcephaly is quite heterogenous; however, a significant number of genes associated with heritable microcephaly and intellectual disability are also associated with centrosome biogenesis and regulation (Thornton and Woods, 2009; Jayaraman et al., 2018; Robinson et al., 2020). Our study implicates Orb2 at the intersection of these pathways.

bioRxiv preprint doi: https://doi.org/10.1101/2021.11.23.469707; this version posted November 23, 2021. The copyright holder for this preprint (which was not certified by peer review) is the author/funder, who has granted bioRxiv a license to display the preprint in perpetuity. It is made available under aCC-BY-NC 4.0 International license.

Materials and Methods

Fly Stocks

The following strains and transgenic lines were used: y^1w^{1118} (Bloomington *Drosophila* Stock Center (BDSC) #1495) was used as the WT control unless otherwise noted. *orb2* brains were isolated from the homozygous null allele, $orb2^{\Delta 36}$ (gift from P. Schedl, Princeton University (Xu et al., 2012)). NSC-specific depletion of *orb2* by $orb2^{RNAi}$ ($P\{TRiP.HMJ22715\}^{attP40}$; BDSC #60424) was driven by $(P\{wor.GAL4.A\}^2$; BDSC #56555). All strains were maintained on Bloomington formula cornmeal-agar media (Lab-Express, Inc.; Ann Arbor, MI) at 25°C in a light and temperature-controlled incubator.

Immunofluorescence

Crawling third instar larva were used for dissections. Larval brains were prepared for immunofluorescence as previously described (Lerit et al., 2014). Briefly, brains were dissected in Schneider's *Drosophila* Medium (ThermoFisher Scientific, #21720024), fixed in 9% paraformaldehyde for 15 min, blocked in PBT buffer (Phosphate Buffered Saline (PBS) supplemented with 1% BSA and 0.1% Tween-20) for one hour at room temperature prior to overnight incubation in primary antibodies in PBT with nutation at 4°C. Samples were further blocked with modified PBT (2% BSA, 0.1% Tween-20, and 4% normal goat serum in PBS) for 1 hour before incubation for two hours at room temperature with secondary antibody and DAPI. Brains were oriented and mounted in Aqua-Poly/Mount (Polysciences, Inc) prior to imaging.

The following primary antibodies were used: guinea pig anti-Asl (1:4000, gift from G. Rogers, University of Arizona), mouse anti-GTU88 (γTub; 1:250–350, Sigma T6557), rabbit anti-Cnn (1:4000 gift from Tim Megraw, Florida State University), guinea pig anti-PLP (1:4000, gift from Nasser Rusan, NIH), rabbit anti-phospho-Histone H3 Ser10 (pH3; 1:2000, Sigma-Millipore, 05-570), mouse anti-β-Tub (clone E7, 1:250; Developmental Studies Hybridoma Bank (DSHB)),

bioRxiv preprint doi: https://doi.org/10.1101/2021.11.23.469707; this version posted November 23, 2021. The copyright holder for this preprint (which was not certified by peer review) is the author/funder, who has granted bioRxiv a license to display the preprint in perpetuity. It is made available under aCC-BY-NC 4.0 International license.

mouse anti-Orb2 (undiluted 1:1 mix of clones 2D11 and 4G8 (DSHB); (Xu et al., 2012)), rat anti-Mira (1:500, Abcam, ab197788), rabbit anti-Baz (1:2000, gift from A. Harris, University of Toronto), rat anti-Dpn (1:500, Abcam, ab195173), rabbit anti-cleaved Caspase 3 (CC3, 1:75; Cell Signaling Technology, 9661s), and mouse anti-Pros (clone MR1A, 1:500; DSHB). Secondary antibodies: Alexa Fluor 488, 568, and 647 (1:500, Molecular Probes). DAPI (ThermoFisher Scientific) was used at 10 ng/mL.

Microscopy

Images were acquired on a Nikon Ti-E inverted microscope fitted with a Yokogawa CSU-X1 spinning disk head (Yokogawa Corp. of America), Orca Flash 4.0 v2 CMOS camera (Hamamatsu Corp.), Perfect Focus system (Nikon), and a Nikon LU-N4 solid-state laser launch (15 mW; 405, 488, 561, and 647 nm) using the following Nikon objectives: 100x 1.49-NA Apo Total Internal Reflection Fluorescence oil immersion, 40x 1.3-NA Plan Fluor oil immersion, and 2x× 0.75-NA Plan Apo. Images were acquired at 25°C through Nikon Elements AR software on a 64-bit HP Z440 workstation (Hewlett-Packard).

Image analysis

Images were assembled using Fiji (National Institutes of Health;(Schindelin et al., 2012)), Adobe Photoshop, and Adobe Illustrator software to separate or merge channels, crop regions of interest, generate maximum-intensity projections, and adjust brightness and contrast.

Centrosome asymmetry

Interphase NSCs were identified by the absence of pH3, round nuclear morphology, and presence of duplicated centrosomes in large (≥10 μm) cells. To blind the experimenter to genotype, maximum projected images were generated, randomized, and used to measure background-subtracted integrated densities from regions of interest (ROIs) centered at the

bioRxiv preprint doi: https://doi.org/10.1101/2021.11.23.469707; this version posted November 23, 2021. The copyright holder for this preprint (which was not certified by peer review) is the author/funder, who has granted bioRxiv a license to display the preprint in perpetuity. It is made available under aCC-BY-NC 4.0 International license.

apical or basal centrosomes. Apical centrosome integrated density (*A*) and basal centrosome integrated density (*B*) were used to calculate the asymmetry index, (*A*-*B*)/(*A*+*B*) ((Lerit and Rusan, 2013)). The data were then unblinded and mean ± S.D. were calculated per genotype.

Polarity, NSC number, and mitotic index

Mitotic NSCs were identified by the presence of pH3 in large, Mira+ cells. To score polarity, maximum projected images were anonymized to blind the experimenter to genotype, and each NSC was scored for the absence or presence of Baz or Mira crescents at the apical or basal cortices, respectively. All Mira+ NSCs were counted to calculate the number of NSCs per optic lobe. Mitotic index is defined as the number of Mira+, pH3+ NSCs per total Mira+ NSCs.

Spindle morphology

Z-stack images of mitotic NSCs labeled with anti-β-Tub to label the mitotic spindle, Asl to mark the centrioles, and Baz to label the apical polarity axis were randomized to blind the experimenter to genotype. The point tool in Fiji was used to record the X,Y, and Z coordinates of four ROIs per cell: 1) center of the apical centrosome, 2) center of the basal centrosome, 3) center of the Baz apical crescent, and 4) center of the DAPI+ condensed chromosomes. These points were used to calculate four different vectors, and vector analysis was used to calculate the angles between specified vectors. The following angles (θ) were calculated: θ_1= *spindle orientation*, the angle between the vectors defined by points 1 and 2 (division axis) relative to points 3 and 4 (polarity axis); θ_2= *apical polarity alignment* is the angle between the vectors defined by points 3 and 4 (apical polarity axis) relative to points 1 and 4 (apical centrosome axis); and θ_3= *centrosome alignment* is the angle between the vectors defined by points 1 and 4 (apical centrosome axis) relative to points 2 and 4 (basal centrosome axis). Angles that fell

bioRxiv preprint doi: https://doi.org/10.1101/2021.11.23.469707; this version posted November 23, 2021. The copyright holder for this preprint (which was not certified by peer review) is the author/funder, who has granted bioRxiv a license to display the preprint in perpetuity. It is made available under aCC-BY-NC 4.0 International license.

outside ± 2 S.D. from the control mean were defined as defective. For spindle alignment, NSCs with spindle angles >75° were classified as orthogonal.

Age-matched brain volume

To age match larva, 20 female virgins and 10 males of the appropriate genotype were allowed to seed a vial for 24 hrs. After removal of the adults, vials were incubated at 25 °C until crawling third instar larva emerged. *orb2* null progeny showed a developmental delay of 24-48 hrs as compared to controls; null larva took ~7-8 days to emerge. Age-matched crawling third instar larva were dissected and prepared for immunofluorescence. The entire volume of the DAPI-labeled brain was imaged. Imaris software (Oxford Instruments) was used to select an ROI of the optic lobe and measure the volume using the 3D surfaces tool (Link et al., 2019).

NSC differentiation and death rate

NSCs were identified by the presence of Dpn. To score for premature differentiation, maximum projected images of Dpn and Pros stained brains were randomized to blind the experimenter to genotype, and an ROI of the central brain region was used to calculate the Pearson's Correlation Coefficient on background-subtracted and automatic threshold–masked images using the Coloc 2 plugin for Fiji (Schindelin et al., 2012). To score cell death, a similar analysis was run on Dpn and CC3 stained brains. To assess specificity of overlapping signals for both experiments, the red channel (Pros or CC3) was rotated 90° clockwise, and colocalization was remeasured.

Immunoblotting

Larval brain extracts were prepared from 20 crawling third instar larva dissected in Schneider's medium, removed of imaginal discs, transferred to fresh media, then rinsed once in cold PBST. Samples were homogenized on ice in 30 μL of fresh PBST using a cordless motor and plastic,

bioRxiv preprint doi: https://doi.org/10.1101/2021.11.23.469707; this version posted November 23, 2021. The copyright holder for this preprint (which was not certified by peer review) is the author/funder, who has granted bioRxiv a license to display the preprint in perpetuity. It is made available under aCC-BY-NC 4.0 International license.

415 disposable homogenizer, supplemented with 20 μL 5x SDS loading buffer, boiled for 10 min at
416 95 °C, then stored at -20 °C or resolved on a commercial 7.5% polyacrylamide gel (Bio-Rad,
417 #4568023. Proteins were transferred to a 0.2 μm nitrocellulose membrane (GE Healthcare) by
418 wet transfer in a buffer containing 25 mM Tris-HCl, pH 7.6, 192 mM glycine, 10% methanol, and
419 0.02% SDS at 4 °C. Membranes were blocked in 5% dry milk in TBST (Tris-buffered saline,
420 0.05% Tween-20), washed well with TBST, and incubated overnight at 4 °C with primary
421 antibodies. After washing with TBST, membranes were incubated for 1.5 hr in secondary
422 antibodies diluted 1:5000 in TBST. Bands were visualized with Clarity ECL substrate (Bio-Rad,
423 1705061) on a Bio-Rad ChemiDoc imaging system.
424 The following primary antibodies were used: rabbit anti-PLP (1:4000, gift from Nasser
425 Rusan, NIH), guinea pig anti-Asl (1:10,000, gift from Greg Rogers, University of Arizona), and
426 mouse anti-Orb2 (1:25 dilution each of 2D11 and 4G8; DSHB, Paul Schedl, Princeton University
427 (Hafer et al., 2011)). Secondary antibodies: goat anti-mouse HRP (1:5000, ThermoFisher
428 #31430), goat anti-rabbit HRP (1:5000, ThermoFisher #31460), and goat anti-guinea pig HRP
429 (1:5000, ThermoFisher #A18769). Densitometry was measured in Adobe Photoshop and
430 protein levels are normalized to the Asl loading control. Full-size, replicated blots are available
431 to view on FigShare: https://doi.org/10.6084/m9.figshare.17052722 . The experiment was
432 repeated with three biological replicates per genotype.
433
434 **Bioinformatics**
435 Gene names were converted to FlyBase identifiers using the Flybase.org tool 'Query by
436 symbols'(Larkin et al., 2021). Overlapping genes were identified by the 'COUNT IF' function in
437 Excel and Venn diagrams were plotted in R-Studio. GO cellular component analysis was done
438 using the Panther statistical overrepresentation test (http://www.pantherdb.org/), and Fisher's

bioRxiv preprint doi: https://doi.org/10.1101/2021.11.23.469707; this version posted November 23, 2021. The copyright holder for this preprint (which was not certified by peer review) is the author/funder, who has granted bioRxiv a license to display the preprint in perpetuity. It is made available under aCC-BY-NC 4.0 International license.

exact test was used to generate an adjusted p-value, i.e., false discovery rate (FDR)(Mi et al., 2021) .

Statistical analysis

Data were plotted and statistical analysis performed using Microsoft Excel, GraphPad Prism, and RStudio software. Normality distributions were determined using a D'Agnostino-Pearson or Shapiro-Wilk normality test. Goodness-of-Fit chi-squared analysis were performed using control distributions as the expected distributions. Data were further analyzed using parametric two-tailed t-test, non-parametric Mann-Whitney test or Kolmogorov-Smirnov (KS) test, or an appropriate post-hoc test as noted in the figure legends. Data are plotted as mean ± S.D. and are representative results from at 2 or more independent experiments.

Supplemental materials

Fig. S1 NSC differentiation and survival in WT vs. *orb2* mutants. Maximum intensity projections of (A) WT and (B) *orb2* brains stained with Dpn (green; NSC nuclei) and CC3 (red; pro-apototic. Insets (boxes) are enlarged to the right to highlight NSCs (dashed ovals). (C) Quantification of the Pearson's correlation coefficient between Dpn and CC3 from N=10 WT and 15 *orb2* optic lobes pooled from two replicates. The CC3 channel was rotated clockwise (90°) to test for specificity of overlapping signals. (D) Maximum intensity projections of WT and (E) *orb2* brains stained with Dpn (green) and Pros (red; differentiated nuclei). (F) Quantification of the Pearson's correlation coefficient between Dpn and Pros from N=16 WT and 18 *orb2* optic lobes pooled from two replicates. The Pros channel was rotated clockwise (90°) to test for specificity of overlapping signals. In (D) and (F), each data point is from one ROI per optic lobe. (G)

bioRxiv preprint doi: https://doi.org/10.1101/2021.11.23.469707; this version posted November 23, 2021. The copyright holder for this preprint (which was not certified by peer review) is the author/funder, who has granted bioRxiv a license to display the preprint in perpetuity. It is made available under aCC-BY-NC 4.0 International license.

Projected images of WT and (H) *orb2* NSCs (dashed ovals) stained for Mira (green; NSCs) and the mitotic marker pH3 (red). (I) Quantification of mitotic index from N=6 WT and 10 *orb2* brains. n.s., not significant by Student's t-test. Bars: (A–E) 20 μm and 8 μm (insets); (G and H) 10 μm.

Fig. S2 Ontological analysis of Orb2 and human CPEB4. A) Venn diagram showing relative transcript pool sizes and overlap detected from the Stepien et al. Orb2 CLIP and Pascual et al. CPEB4 datasets (Stepien et al., 2016; Pascual et al., 2020b). B) Top 5 gene ontologies overrepresented in the overlapping transcripts by lowest raw *p* value. C) Overrepresentation tests for gene ontologies implicated in the centrosome were not significant. D) Overrepresentation test of genes in the Orb2 CLIPseq with BC $\geq$3 yields significant centrosome ontologies. -log *p*-values are plotted with a significance cut-off of p=0.05, noted by the dashed line and asterisk. Genes are listed in Table S1.

Table S1. Orb2 and CPEB4 common RNA targets. Sheet 1 lists FlyBase IDs for all transcripts detected in (Stepien et al., 2016; Pascual et al., 2020b). Sheet 2 lists overlapping genes; column E is sortable to list genes with centrosome ontologies. Sheet 3 lists GO terms overrepresented in the overlapping genes, column J is sortable to list genes with centrosome ontologies. Sheet 4 lists Orb2 targets from (Stepien et al., 2016) with BC $\geq$ 3; column F is sortable to list genes with centrosome ontologies. Sheet 5 shows an overrepresentation test for centrosome ontologies from the Orb2 BC $\geq$ 3 gene list. Sheet 6 lists each gene included in the indicated centrosome ontologies.

Competing interest statement

The authors have no competing interests to declare.

bioRxiv preprint doi: https://doi.org/10.1101/2021.11.23.469707; this version posted November 23, 2021. The copyright holder for this preprint (which was not certified by peer review) is the author/funder, who has granted bioRxiv a license to display the preprint in perpetuity. It is made available under aCC-BY-NC 4.0 International license.

Acknowledgements

We thank Drs. Timothy Megraw, Nasser Rusan, Greg Rogers, and Paul Schedl for gifts of reagents. We are grateful to members of the Lerit lab and Drs. Victor Faundez and Nasser Rusan for constructive feedback on the manuscript.

This work was supported by NIH grant T32GM008490 (BVR), American Heart Association grant 20POST35210023 (to JF), and R01GM138544 (to DAL).

Author contributions

Beverly V. Robinson– data curation, formal analysis, funding acquisition, investigation, methodology, visualization, writing–original draft, and writing–review & editing.

Junnan Fang– formal analysis, funding acquisition, investigation, methodology, and writing–review & editing.

Dipen S. Mehta– investigation

Joseph D. Buehler– formal analysis, software, visualization, and writing–review & editing.

Dorothy A. Lerit– conceptualization, formal analysis, funding acquisition, investigation, methodology, project administration, supervision, visualization, writing–original draft, and writing–review & editing.

bioRxiv preprint doi: https://doi.org/10.1101/2021.11.23.469707; this version posted November 23, 2021. The copyright holder for this preprint (which was not certified by peer review) is the author/funder, who has granted bioRxiv a license to display the preprint in perpetuity. It is made available under aCC-BY-NC 4.0 International license.

References

Abdel-Salam, G.M.H., I.S.M. Sayed, H.H. Afifi, S.F. Abdel-Ghafar, M.R. Abouzaid, S.I. Ismail, M.S. Aglan, M.Y. Issa, H.T. El-Bassyouni, G. El-Kamah, L.K. Effat, M. Eid, M.S. Zaki, S.A. Temtamy, and M.S. Abdel-Hamid. 2020. Microcephalic osteodysplastic primordial dwarfism type II: Additional nine patients with implications on phenotype and genotype correlation. *Am. J. Med. Genet. A*. 182:1407-1420.

Albertson, R., C. Chabu, A. Sheehan, and C.Q. Doe. 2004. Scribble protein domain mapping reveals a multistep localization mechanism and domains necessary for establishing cortical polarity. *J. Cell Sci.* 117:6061-6070.

Atwood, S.X., and K.E. Prehoda. 2009. aPKC phosphorylates Miranda to polarize fate determinants during neuroblast asymmetric cell division. *Curr. Biol.* 19:723-729.

Betschinger, J., K. Mechtler, and J.A. Knoblich. 2003. The Par complex directs asymmetric cell division by phosphorylating the cytoskeletal protein Lgl. *Nature*. 422:326-330.

Bier, E., H. Vaessin, S. Younger-Shepherd, L.Y. Jan, and Y.N. Jan. 1992. deadpan, an essential pan-neural gene in Drosophila, encodes a helix-loop-helix protein similar to the hairy gene product. *Genes Dev.* 6:2137-2151.

Bond, J., E. Roberts, G.H. Mochida, D.J. Hampshire, S. Scott, J.M. Askham, K. Springell, M. Mahadevan, Y.J. Crow, A.F. Markham, C.A. Walsh, and C.G. Woods. 2002. ASPM is a major determinant of cerebral cortical size. *Nat. Genet.* 32:316-320.

Broadus, J., and C.Q. Doe. 1997. Extrinsic cues, intrinsic cues and microfilaments regulate asymmetric protein localization in Drosophila neuroblasts. *Curr. Biol.* 7:827-835.

Cabernard, C., and C.Q. Doe. 2009. Apical/basal spindle orientation is required for neuroblast homeostasis and neuronal differentiation in Drosophila. *Dev. Cell*. 17:134-141.

Cai, Y., F. Yu, S. Lin, W. Chia, and X. Yang. 2003. Apical complex genes control mitotic spindle geometry and relative size of daughter cells in Drosophila neuroblast and pI asymmetric divisions. *Cell*. 112:51-62.

Conduit, P.T., and J.W. Raff. 2010. Cnn dynamics drive centrosome size asymmetry to ensure daughter centriole retention in Drosophila neuroblasts. *Curr. Biol.* 20:2187-2192.

Conduit, P.T., A. Wainman, and J.W. Raff. 2015. Centrosome function and assembly in animal cells. *Nat. Rev. Mol. Cell Biol.* 16:611-624.

Doe, C.Q. 2008. Neural stem cells: balancing self-renewal with differentiation. *Development*. 135:1575-1587.

Doe, C.Q., Q. Chu-LaGraff, D.M. Wright, and M.P. Scott. 1991. The prospero gene specifies cell fates in the Drosophila central nervous system. *Cell*. 65:451-464.

Fan, Y., and A. Bergmann. 2010. The cleaved-Caspase-3 antibody is a marker of Caspase-9-like DRONC activity in Drosophila. *Cell Death Differ.* 17:534-539.

Gallaud, E., A. Ramdas Nair, N. Horsley, A. Monnard, P. Singh, T.T. Pham, D. Salvador Garcia, A. Ferrand, and C. Cabernard. 2020. Dynamic centriolar localization of Polo and Centrobin in early mitosis primes centrosome asymmetry. *PLoS Biol.* 18:e3000762.

Gambarotto, D., C. Pennetier, J.M. Ryniawec, D.W. Buster, D. Gogendeau, A. Goupil, M. Nano, A. Simon, D. Blanc, V. Racine, Y. Kimata, G.C. Rogers, and R. Basto. 2019. Plk4 Regulates Centriole Asymmetry and Spindle Orientation in Neural Stem Cells. *Dev. Cell*. 50:11-24 e10.

Goldstein, B., and I.G. Macara. 2007. The PAR proteins: fundamental players in animal cell polarization. *Dev. Cell*. 13:609-622.

Gould, R.R., and G.G. Borisy. 1977. The pericentriolar material in Chinese hamster ovary cells nucleates microtubule formation. *J Cell Biol*. 73:601-615.

Groisman, I., Y.S. Huang, R. Mendez, Q. Cao, W. Theurkauf, and J.D. Richter. 2000. CPEB, maskin, and cyclin B1 mRNA at the mitotic apparatus: implications for local translational control of cell division. *Cell*. 103:435-447.

bioRxiv preprint doi: https://doi.org/10.1101/2021.11.23.469707; this version posted November 23, 2021. The copyright holder for this preprint (which was not certified by peer review) is the author/funder, who has granted bioRxiv a license to display the preprint in perpetuity. It is made available under aCC-BY-NC 4.0 International license.

562 Hafer, N., S. Xu, K.M. Bhat, and P. Schedl. 2011. The Drosophila CPEB protein Orb2 has a
563 novel expression pattern and is important for asymmetric cell division and nervous
564 system function. *Genetics*. 189:907-921.
565 Hervas, R., L. Li, A. Majumdar, C. Fernandez-Ramirez Mdel, J.R. Unruh, B.D. Slaughter, A.
566 Galera-Prat, E. Santana, M. Suzuki, Y. Nagai, M. Bruix, S. Casas-Tinto, M. Menendez,
567 D.V. Laurents, K. Si, and M. Carrion-Vazquez. 2016. Molecular Basis of Orb2
568 Amyloidogenesis and Blockade of Memory Consolidation. *PLoS Biol.* 14:e1002361.
569 Huang, Y.S., M.C. Kan, C.L. Lin, and J.D. Richter. 2006. CPEB3 and CPEB4 in neurons:
570 analysis of RNA-binding specificity and translational control of AMPA receptor GluR2
571 mRNA. *EMBO J.* 25:4865-4876.
572 Inaba, M., Z.G. Venkei, and Y.M. Yamashita. 2015. The polarity protein Baz forms a platform for
573 the centrosome orientation during asymmetric stem cell division in the Drosophila male
574 germline. *Elife*. 4.
575 Januschke, J., and C. Gonzalez. 2010. The interphase microtubule aster is a determinant of
576 asymmetric division orientation in Drosophila neuroblasts. *J Cell Biol*. 188:693-706.
577 Januschke, J., S. Llamazares, J. Reina, and C. Gonzalez. 2011. Drosophila neuroblasts retain
578 the daughter centrosome. *Nat Commun*. 2:243.
579 Januschke, J., J. Reina, S. Llamazares, T. Bertran, F. Rossi, J. Roig, and C. Gonzalez. 2013.
580 Centrobin controls mother-daughter centriole asymmetry in Drosophila neuroblasts. *Nat.*
581 *Cell Biol.* 15:241-248.
582 Jayaraman, D., B.I. Bae, and C.A. Walsh. 2018. The Genetics of Primary Microcephaly. *Annu*
583 *Rev Genomics Hum Genet*. 19:177-200.
584 Kacsoh, B.Z., J. Bozler, S. Hodge, M. Ramaswami, and G. Bosco. 2015. A novel paradigm for
585 nonassociative long-term memory in Drosophila: predator-induced changes in
586 oviposition behavior. *Genetics*. 199:1143-1157.
587 Keleman, K., S. Kruttner, M. Alenius, and B.J. Dickson. 2007. Function of the Drosophila CPEB
588 protein Orb2 in long-term courtship memory. *Nat. Neurosci.* 10:1587-1593.
589 Khan, M.R., L. Li, C. Perez-Sanchez, A. Saraf, L. Florens, B.D. Slaughter, J.R. Unruh, and K.
590 Si. 2015. Amyloidogenic Oligomerization Transforms Drosophila Orb2 from a Translation
591 Repressor to an Activator. *Cell*. 163:1468-1483.
592 Khodjakov, A., and C.L. Rieder. 1999. The sudden recruitment of gamma-tubulin to the
593 centrosome at the onset of mitosis and its dynamic exchange throughout the cell cycle,
594 do not require microtubules. *J Cell Biol*. 146:585-596.
595 Knoblich, J.A. 2008. Mechanisms of asymmetric stem cell division. *Cell*. 132:583-597.
596 Knoblich, J.A., L.Y. Jan, and Y.N. Jan. 1995. Asymmetric segregation of Numb and Prospero
597 during cell division. *Nature*. 377:624-627.
598 Kraut, R., W. Chia, L.Y. Jan, Y.N. Jan, and J.A. Knoblich. 1996. Role of inscuteable in orienting
599 asymmetric cell divisions in Drosophila. *Nature*. 383:50-55.
600 Kruttner, S., B. Stepien, J.N. Noordermeer, M.A. Mommaas, K. Mechtler, B.J. Dickson, and K.
601 Keleman. 2012. Drosophila CPEB Orb2A mediates memory independent of Its RNA-
602 binding domain. *Neuron*. 76:383-395.
603 Kuchinke, U., F. Grawe, and E. Knust. 1998. Control of spindle orientation in Drosophila by the
604 Par-3-related PDZ-domain protein Bazooka. *Curr. Biol.* 8:1357-1365.
605 Lai, S.L., and C.Q. Doe. 2014. Transient nuclear Prospero induces neural progenitor
606 quiescence. *Elife*. 3.
607 Larkin, A., S.J. Marygold, G. Antonazzo, H. Attrill, G. Dos Santos, P.V. Garapati, J.L. Goodman,
608 L.S. Gramates, G. Millburn, V.B. Strelets, C.J. Tabone, J. Thurmond, and C. FlyBase.
609 2021. FlyBase: updates to the Drosophila melanogaster knowledge base. *Nucleic Acids*
610 *Res.* 49:D899-D907.
611 Lerit, D.A., K.M. Plevock, and N.M. Rusan. 2014. Live imaging of Drosophila larval neuroblasts.
612 *J Vis Exp*.

bioRxiv preprint doi: https://doi.org/10.1101/2021.11.23.469707; this version posted November 23, 2021. The copyright holder for this preprint (which was not certified by peer review) is the author/funder, who has granted bioRxiv a license to display the preprint in perpetuity. It is made available under aCC-BY-NC 4.0 International license.

Lerit, D.A., and N.M. Rusan. 2013. PLP inhibits the activity of interphase centrosomes to ensure their proper segregation in stem cells. *J Cell Biol*. 202:1013-1022.

Licatalosi, D.D., A. Mele, J.J. Fak, J. Ule, M. Kayikci, S.W. Chi, T.A. Clark, A.C. Schweitzer, J.E. Blume, X. Wang, J.C. Darnell, and R.B. Darnell. 2008. HITS-CLIP yields genome-wide insights into brain alternative RNA processing. *Nature*. 456:464-469.

Link, N., H. Chung, A. Jolly, M. Withers, B. Tepe, B.R. Arenkiel, P.S. Shah, N.J. Krogan, H. Aydin, B.B. Geckinli, T. Tos, S. Isikay, B. Tuysuz, G.H. Mochida, A.X. Thomas, R.D. Clark, G.M. Mirzaa, J.R. Lupski, and H.J. Bellen. 2019. Mutations in ANKLE2, a ZIKA Virus Target, Disrupt an Asymmetric Cell Division Pathway in Drosophila Neuroblasts to Cause Microcephaly. *Dev. Cell*. 51:713-729 e716.

Mastushita-Sakai, T., E. White-Grindley, J. Samuelson, C. Seidel, and K. Si. 2010. Drosophila Orb2 targets genes involved in neuronal growth, synapse formation, and protein turnover. *Proc. Natl. Acad. Sci. U. S. A.* 107:11987-11992.

Mi, H., D. Ebert, A. Muruganujan, C. Mills, L.P. Albou, T. Mushayamaha, and P.D. Thomas. 2021. PANTHER version 16: a revised family classification, tree-based classification tool, enhancer regions and extensive API. *Nucleic Acids Res.* 49:D394-D403.

Pascual, R., J. Martin, F. Salvador, O. Reina, V. Chanes, A. Millanes-Romero, C. Suner, G. Fernandez-Miranda, A. Bartomeu, Y.S. Huang, R.R. Gomis, and R. Mendez. 2020a. The RNA binding protein CPEB2 regulates hormone sensing in mammary gland development and luminal breast cancer. *Sci Adv*. 6:eaax3868.

Pascual, R., C. Segura-Morales, M. Omerzu, N. Bellora, E. Belloc, C.L. Castellazzi, O. Reina, E. Eyras, M.M. Maurice, A. Millanes-Romero, and R. Mendez. 2020b. mRNA spindle localization and mitotic translational regulation by CPEB1 and CPEB4. *RNA*.

Ramdas Nair, A., P. Singh, D. Salvador Garcia, D. Rodriguez-Crespo, B. Egger, and C. Cabernard. 2016. The Microcephaly-Associated Protein Wdr62/CG7337 Is Required to Maintain Centrosome Asymmetry in Drosophila Neuroblasts. *Cell Rep.* 14:1100-1113.

Rebollo, E., P. Sampaio, J. Januschke, S. Llamazares, H. Varmark, and C. Gonzalez. 2007. Functionally unequal centrosomes drive spindle orientation in asymmetrically dividing Drosophila neural stem cells. *Dev. Cell*. 12:467-474.

Robinson, B.V., V. Faundez, and D.A. Lerit. 2020. Understanding microcephaly through the study of centrosome regulation in Drosophila neural stem cells. *Biochem. Soc. Trans.* 48:2101-2115.

Rolls, M.M., R. Albertson, H.P. Shih, C.Y. Lee, and C.Q. Doe. 2003. Drosophila aPKC regulates cell polarity and cell proliferation in neuroblasts and epithelia. *J Cell Biol*. 163:1089-1098.

Rusan, N.M., and M. Peifer. 2007. A role for a novel centrosome cycle in asymmetric cell division. *J Cell Biol*. 177:13-20.

Sanguanini, M., and A. Cattaneo. 2018. A continuous model of physiological prion aggregation suggests a role for Orb2 in gating long-term synaptic information. *R Soc Open Sci*. 5:180336.

Schindelin, J., I. Arganda-Carreras, E. Frise, V. Kaynig, M. Longair, T. Pietzsch, S. Preibisch, C. Rueden, S. Saalfeld, B. Schmid, J.Y. Tinevez, D.J. White, V. Hartenstein, K. Eliceiri, P. Tomancak, and A. Cardona. 2012. Fiji: an open-source platform for biological-image analysis. *Nat Methods*. 9:676-682.

Shen, C.P., J.A. Knoblich, Y.M. Chan, M.M. Jiang, L.Y. Jan, and Y.N. Jan. 1998. Miranda as a multidomain adapter linking apically localized Inscuteable and basally localized Staufen and Prospero during asymmetric cell division in Drosophila. *Genes Dev.* 12:1837-1846.

Siegrist, S.E., and C.Q. Doe. 2005. Microtubule-induced Pins/Galphai cortical polarity in Drosophila neuroblasts. *Cell*. 123:1323-1335.

Siegrist, S.E., and C.Q. Doe. 2006. Extrinsic cues orient the cell division axis in Drosophila embryonic neuroblasts. *Development*. 133:529-536.

bioRxiv preprint doi: https://doi.org/10.1101/2021.11.23.469707; this version posted November 23, 2021. The copyright holder for this preprint (which was not certified by peer review) is the author/funder, who has granted bioRxiv a license to display the preprint in perpetuity. It is made available under aCC-BY-NC 4.0 International license.

Siller, K.H., C. Cabernard, and C.Q. Doe. 2006. The NuMA-related Mud protein binds Pins and regulates spindle orientation in Drosophila neuroblasts. *Nat. Cell Biol.* 8:594-600.

Singh, P., A. Ramdas Nair, and C. Cabernard. 2014. The centriolar protein Bld10/Cep135 is required to establish centrosome asymmetry in Drosophila neuroblasts. *Curr. Biol.* 24:1548-1555.

Stepien, B.K., C. Oppitz, D. Gerlach, U. Dag, M. Novatchkova, S. Kruttner, A. Stark, and K. Keleman. 2016. RNA-binding profiles of Drosophila CPEB proteins Orb and Orb2. *Proc. Natl. Acad. Sci. U. S. A.* 113:E7030-E7038.

Thornton, G.K., and C.G. Woods. 2009. Primary microcephaly: do all roads lead to Rome? *Trends Genet.* 25:501-510.

Vaessin, H., E. Grell, E. Wolff, E. Bier, L.Y. Jan, and Y.N. Jan. 1991. prospero is expressed in neuronal precursors and encodes a nuclear protein that is involved in the control of axonal outgrowth in Drosophila. *Cell*. 67:941-953.

Varmark, H., S. Llamazares, E. Rebollo, B. Lange, J. Reina, H. Schwarz, and C. Gonzalez. 2007. Asterless is a centriolar protein required for centrosome function and embryo development in Drosophila. *Curr. Biol.* 17:1735-1745.

Wang, C., S. Li, J. Januschke, F. Rossi, Y. Izumi, G. Garcia-Alvarez, S.S. Gwee, S.B. Soon, H.K. Sidhu, F. Yu, F. Matsuzaki, C. Gonzalez, and H. Wang. 2011. An ana2/ctp/mud complex regulates spindle orientation in Drosophila neuroblasts. *Dev. Cell*. 21:520-533.

Wodarz, A., and W.B. Huttner. 2003. Asymmetric cell division during neurogenesis in Drosophila and vertebrates. *Mech. Dev.* 120:1297-1309.

Xu, S., N. Hafer, B. Agunwamba, and P. Schedl. 2012. The CPEB protein Orb2 has multiple functions during spermatogenesis in Drosophila melanogaster. *PLoS Genet*. 8:e1003079.

Yu, F., Y. Cai, R. Kaushik, X. Yang, and W. Chia. 2003. Distinct roles of Galphai and Gbeta13F subunits of the heterotrimeric G protein complex in the mediation of Drosophila neuroblast asymmetric divisions. *J Cell Biol*. 162:623-633.

bioRxiv preprint doi: https://doi.org/10.1101/2021.11.23.469707; this version posted November 23, 2021. The copyright holder for this preprint (which was not certified by peer review) is the author/funder, who has granted bioRxiv a license to display the preprint in perpetuity. It is made available under aCC-BY-NC 4.0 International license.

692 **Abbreviations used:**
693
694 ACD, asymmetric cell division
695 AI, asymmetry index
696 Asl, Asterless
697 Baz, Bazooka/PAR-3
698 BC, biologic complexity
699 Cep135, Centrosomal protein 135kDa
700 Cnb, Centrobin
701 Cnn, Centrosomin
702 γTub, γ-Tubulin
703 GMC, ganglion mother cell
704 Mira, Miranda
705 MT, microtubule
706 MTOC, microtubule-organizing center
707 NSC, neural stem cell
708 PCM, pericentriolar material
709 PLP, Pericentrin-like protein
710 Polo, Polo kinase
711 Wdr62, WD repeat domain 62
712 *w*or, *worniu*
713 WT, wild-type
714

715

716 **Figure Legends**

717 **Figure 1. Orb2 contributes to centrosome asymmetry.** Maximum intensity projections of

718 interphase NSCs (dashed circles) stained for Asl (centrioles, magenta) and γTub (PCM, cyan).

719 Solid and dashed boxes mark apical vs. basal centrosomes; enlarged at right. (A) WT NSC with

720 γTub enriched at the apical centrosome. (B) *orb2* NSC with γTub at both centrosomes. (C) AIs

721 of Asl and γTub in N=30 NSCs from n=8 WT brains and N=40 NSCs from n=10 *orb2* brains.

722 Each dot is a measurement from one cell. (D) Frequency distribution of Asl and γTub AIs in WT

723 vs. *orb2* NSCs. Light grey (outlier) values are > 2 S.D. from the control mean. (E) Scatter plot of

724 γTub levels at apical vs. basal centrosomes in N=24 NSCs from n=8 WT brains and N=10

725 symmetrized NSCs from n=7 *orb2* brains (defined as AI >2 S.D. from WT mean). (F) no *GAL4*

726 control NSCs resemble WT. (G) $orb2^{RNAi}$ NSC with γTub at both centrosomes. (H) AIs from

727 N=39 NSCs from n=6 no GAL4 brains and N=51 NSC from n=6 $orb2^{RNAi}$ brains. (I) Frequency

bioRxiv preprint doi: https://doi.org/10.1101/2021.11.23.469707; this version posted November 23, 2021. The copyright holder for this preprint (which was not certified by peer review) is the author/funder, who has granted bioRxiv a license to display the preprint in perpetuity. It is made available under aCC-BY-NC 4.0 International license.

distribution of Asl and γTub AIs in control vs. *orb2*^{RNAi} brains. (J) Scatter plot of γTub at centrosomes from N=39 NSCs from n=6 control brains and N=16 NSCs from n=6 *worGAL4>orb2*^{RNAi} brains. Mean ± SD displayed. The experiments were repeated ≥3 independent replicates and significance determined by (C, H) Kolmogorov-Smirnov test, (D, I) chi-square test, (E, J) Mann-Whitney test: n.s., not significant; *, $p \leq 0.05$; **$p \leq 0.01$ ***, $p<0.001$; and ****, $p<0.0001$. Bars: 5 μm, 1 μm (insets).

Figure 2. Orb2 is required for centrosome segregation and spindle morphogenesis. Maximum intensity projections of interphase NSCs (dashed circles) from (A) WT, (B) *orb2*, (D) no *GAL4* control, and (E) *orb2*^{RNAi} stained for Asl (arrows). Solid and dashed boxes mark apical vs. basal centrosomes; enlarged at right. (C and F) Frequency distributions of supernumerary centrosomes in interphase NSCs. (G) WT and (H) *orb2* NSCs stained for Baz (apical cortex, cyan), pH3 (mitotic, cyan), Mira (basal cortex, magenta), and Asl (yellow; arrowheads). (I) Frequency distribution of apical Baz and/or basal Mira crescents in mitotic NSCs. (J) Cartoon depicts points used to measure within mitotic NSCs: θ_1 spindle orientation, θ_2 apical polarity alignment, and θ_3 centrosome alignment (*Methods*). (K) WT and (L) *orb2* NSCs stained for MTs (β-Tub, magenta), Asl (yellow), Baz (cyan), and DAPI (DNA, grey). (M) Plot and (N) frequency distribution of θ_1 spindle orientation. (O) Plot and (P) frequency distribution of θ_2 apical polarity alignment. (Q) Plot and (R) frequency distribution of θ_3 centrosome alignment from N=33 WT and N=32 *orb2* mitotic NSCs from a single experiment across two replicates. Light grey θ are >2 SD from the WT mean. Mean ± SD indicated; significance determined by (C, F, I, N, P, R) Chi-squared test or (M, O, Q) Two-tailed t-test. n.s., not significant; *, $p<0.05$; and ****, $p<0.0001$. Bars: 5 μm; 1 μm (insets).

bioRxiv preprint doi: https://doi.org/10.1101/2021.11.23.469707; this version posted November 23, 2021. The copyright holder for this preprint (which was not certified by peer review) is the author/funder, who has granted bioRxiv a license to display the preprint in perpetuity. It is made available under aCC-BY-NC 4.0 International license.

752 **Figure 3. NSC-autonomous and non-autonomous Orb2 activities support**
753 **neurodevelopment.** Projected third instar larval optic lobes (dashed lines) stained for DAPI or
754 Mira. In age-matched brains, (A) WT are larger than (B) *orb2* and (C) WT have more NSCs than
755 (D) *orb2*. (E) Volume quantified from N=15 WT and 13 *orb2* brains. (F) Quantification of NSCs in
756 N=6 WT and 10 *orb2* brains. In age-matched brains, (G) no *GAL4* controls are sized as (H)
757 $orb2^{RNAi}$ brains. Yet, (I) no *GAL4* controls have more NSCs than (J) $orb2^{RNAi}$. (K) Volume and (L)
758 NSC counts quantified from N=6 brains per genotype. Brain volumes were measured from one
759 lobe per brain and normalized to the control mean (Link et al., 2019). Mean ± SD displayed.
760 Significance determined by Student's t-test: n.s., not significant; *, p<0.05***; and p<0.001.
761 Bars: 40 μm.
762
763 **Figure 4. Orb2 localizes to active NSC centrosomes.** (A) Maximum-intensity projections of
764 WT NSCs (dashed circles) stained for Asl (magenta), Cnn (PCM; yellow), and Orb2 (cyan).
765 Solid and dashed boxes note apical vs. basal centrosomes; enlarged at right. (B) Orb2 AI and
766 (C) Orb2 levels on apical vs. basal centrosomes quantified from N=24 late interphase NSCs.
767 Mean ± SD displayed; **, p=0.003 by Welch's t-test. Bars: 5 μm, 1 μm (inset).
768
769 **Figure 5. Orb2 regulates PLP protein levels.** (A) Immunoblot of PLP, Asl, and Orb2 proteins
770 from WT and *orb2* third instar larval brain extracts. (B) Normalized (to Asl) relative PLP levels in
771 WT and *orb2* larval brains from 3 biological replicates. (C) Max projected WT and *orb2* NSCs
772 (dashed circles) stained for γTub (magenta) and PLP (cyan). Solid and dashed boxes note
773 apical vs. basal centrosomes; enlarged at right. (D) PLP AI calculated from N=24 WT and 32
774 *orb2* interphase NSCs. (E) PLP localization to apical and basal centrosomes in N=24 WT vs.
775 N=43 *orb2* interphase NSCs. Data representative from a single experiment across 2 replicates.
776 (F) Model depicts NSC-autonomous function of Orb2 to support interphase centrosome
777 asymmetry and NSC-independent requirement for normal brain volume. Loss of *orb2* activity

bioRxiv preprint doi: https://doi.org/10.1101/2021.11.23.469707; this version posted November 23, 2021. The copyright holder for this preprint (which was not certified by peer review) is the author/funder, who has granted bioRxiv a license to display the preprint in perpetuity. It is made available under aCC-BY-NC 4.0 International license.

778 (grey cells) impairs basal centrosome inactivation (PCM, green). Centrosome-localized Orb2
779 (WT apical; *top box*) enhances centrosome activation, perhaps by translational activation of one
780 or more targets (black, Orb2 target BC≥3; see Table S1). Conversely, cytoplasmic Orb2
781 supports basal centrosome inactivation (*bottom box*), required for centrosome separation,
782 spindle orientation, and centrosome segregation to the daughter cells. Mean ± SD displayed; *,
783 $p<0.05$ by unpaired, one-tailed t-test; n.s., not significant. Uncropped, replicated blots are
784 available to view: https://doi.org/10.6084/m9.figshare.17052722 Bars: 5 μm; insets 1 μm.
785
786

bioRxiv preprint doi: https://doi.org/10.1101/2021.11.23.469707; this version posted November 23, 2021. The copyright holder for this preprint (which was not certified by peer review) is the author/funder, who has granted bioRxiv a license to display the preprint in perpetuity. It is made available under aCC-BY-NC 4.0 International license.

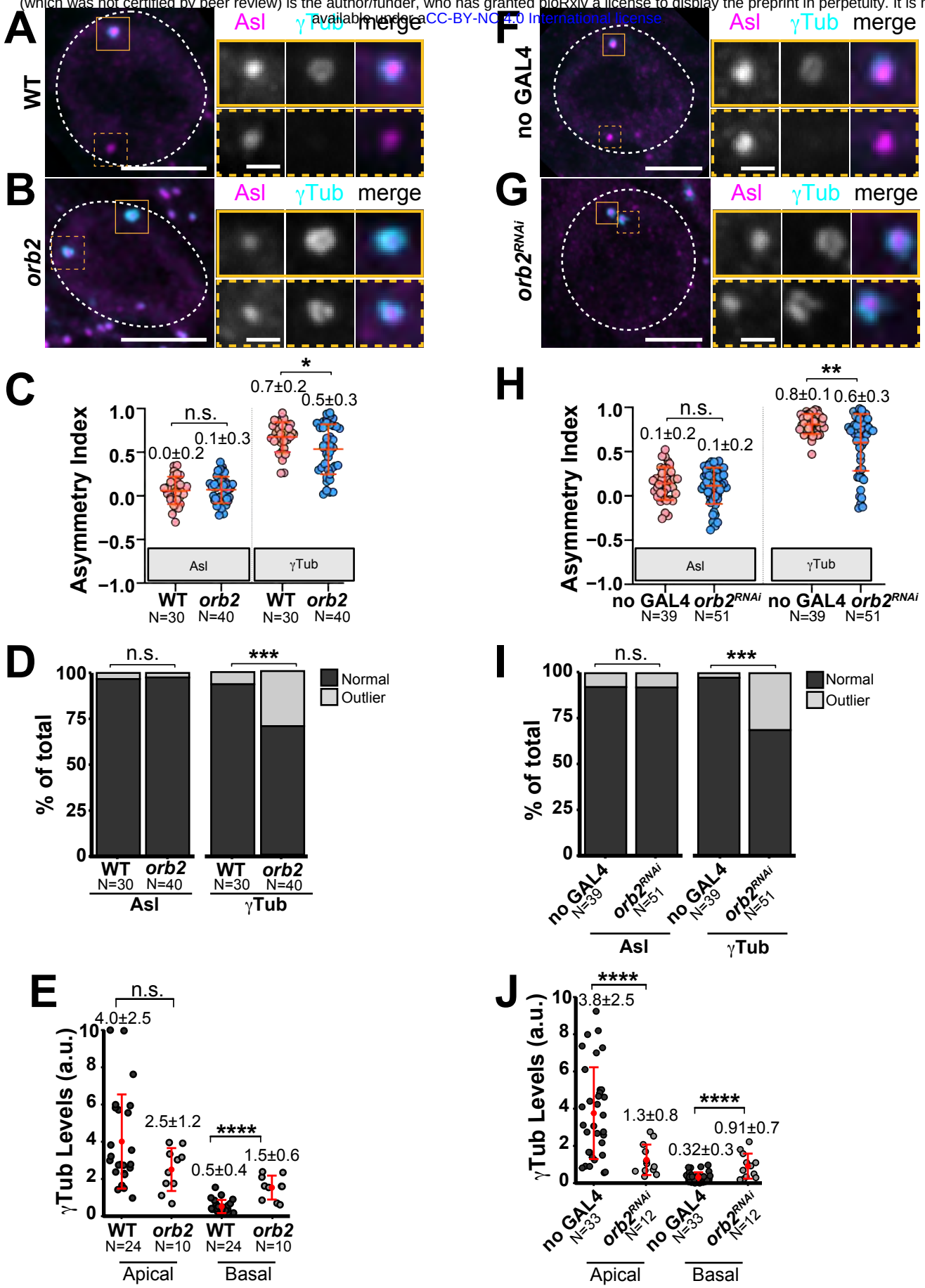

Robinson and Lerit Figure 1. orb2 is required for centrosome asymmetry

bioRxiv preprint doi: https://doi.org/10.1101/2021.11.23.469707; this version posted November 23, 2021. The copyright holder for this preprint (which was not certified by peer review) is the author/funder, who has granted bioRxiv a license to display the preprint in perpetuity. It is made available under aCC-BY-NC 4.0 International license.

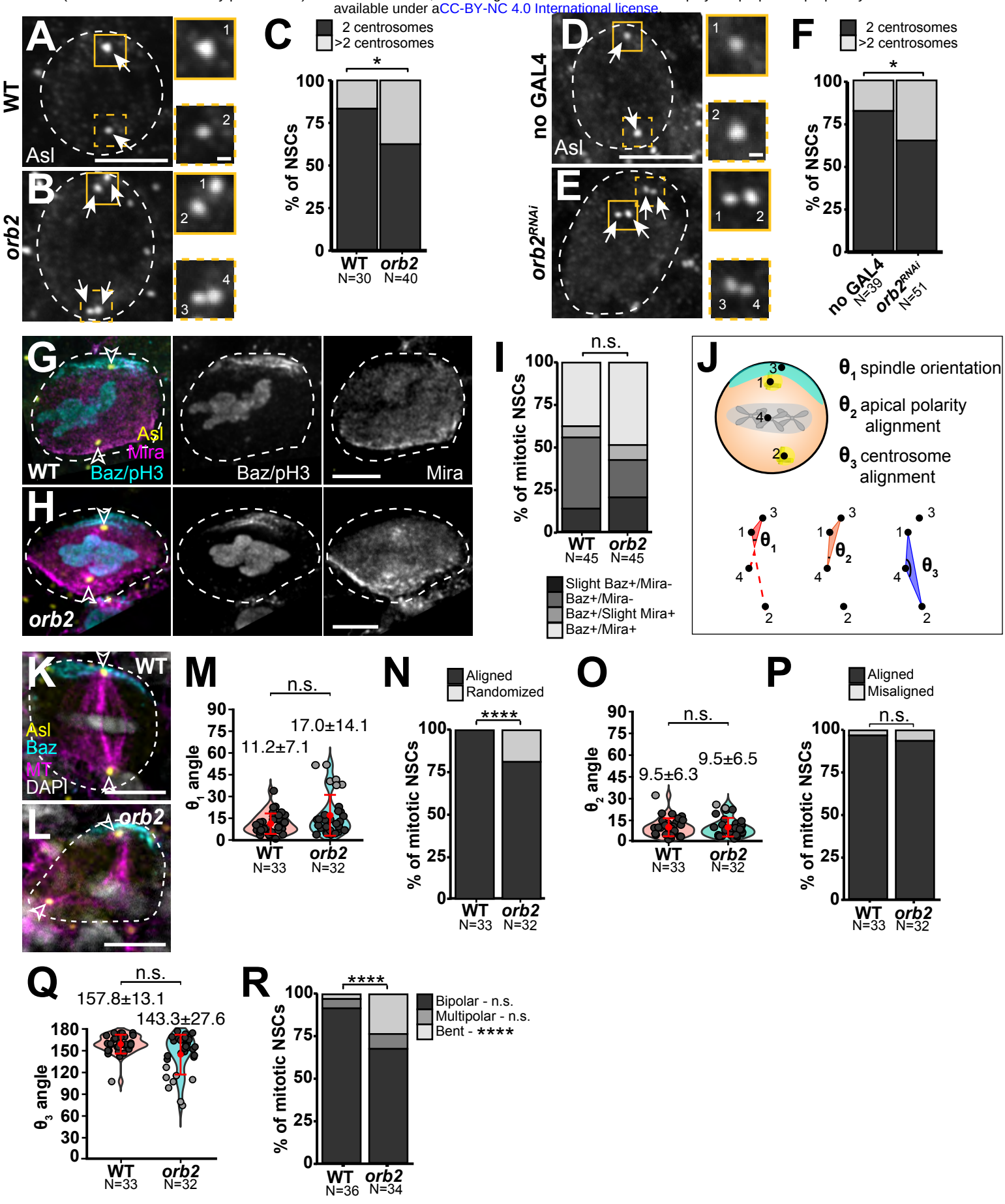

Robinson et al.

Figure 2. Orb2 is required for centrosome segregation and spindle morphogenesis

bioRxiv preprint doi: https://doi.org/10.1101/2021.11.23.469707; this version posted November 23, 2021. The copyright holder for this preprint (which was not certified by peer review) is the author/funder, who has granted bioRxiv a license to display the preprint in perpetuity. It is made available under aCC-BY-NC 4.0 International license.

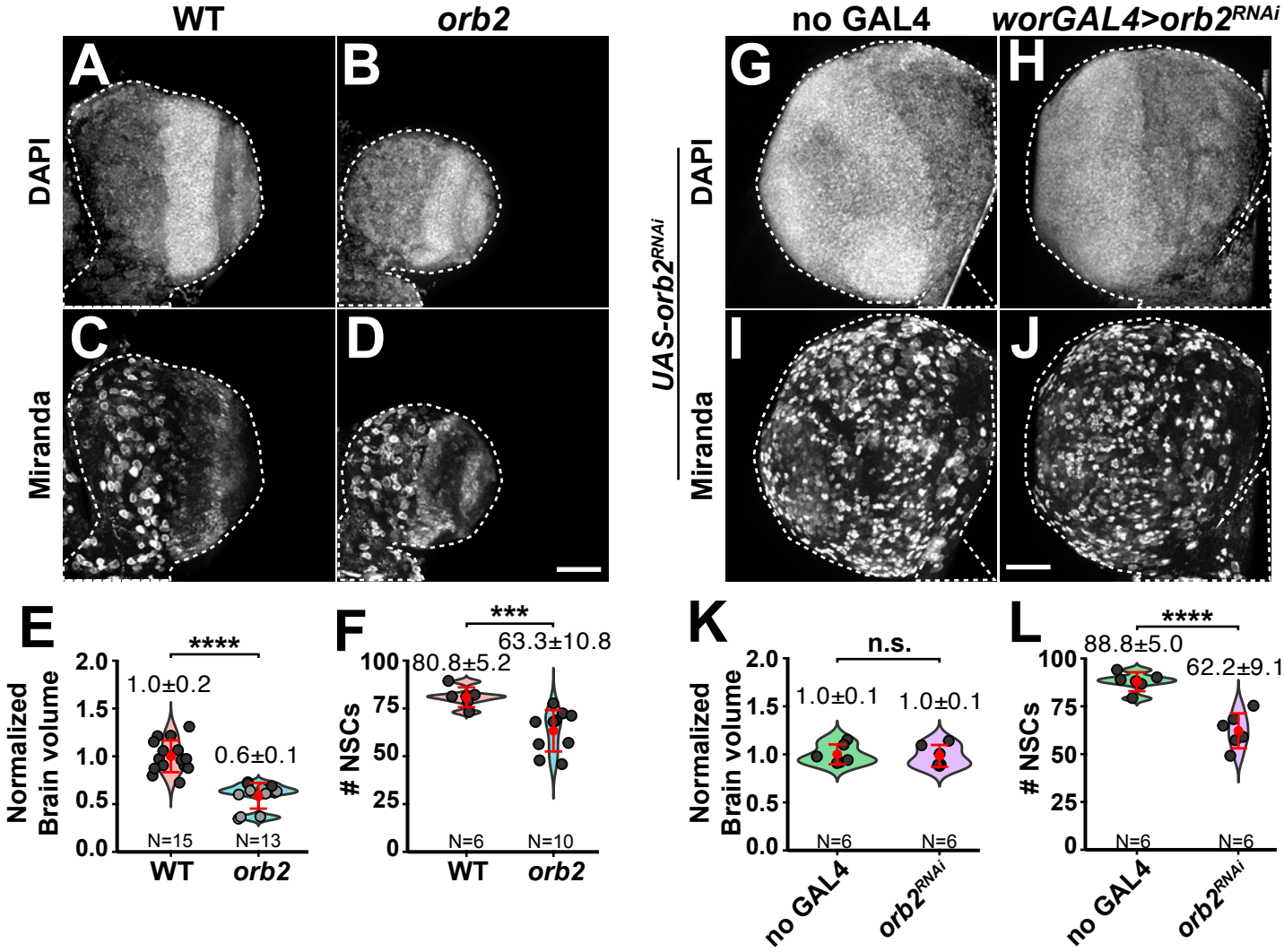

Robinson et al.

Figure 3. NSC-autonomous and non-autonomous Orb2 activities support neurodevelopment

bioRxiv preprint doi: https://doi.org/10.1101/2021.11.23.469707; this version posted November 23, 2021. The copyright holder for this preprint (which was not certified by peer review) is the author/funder, who has granted bioRxiv a license to display the preprint in perpetuity. It is made available under aCC-BY-NC 4.0 International license.

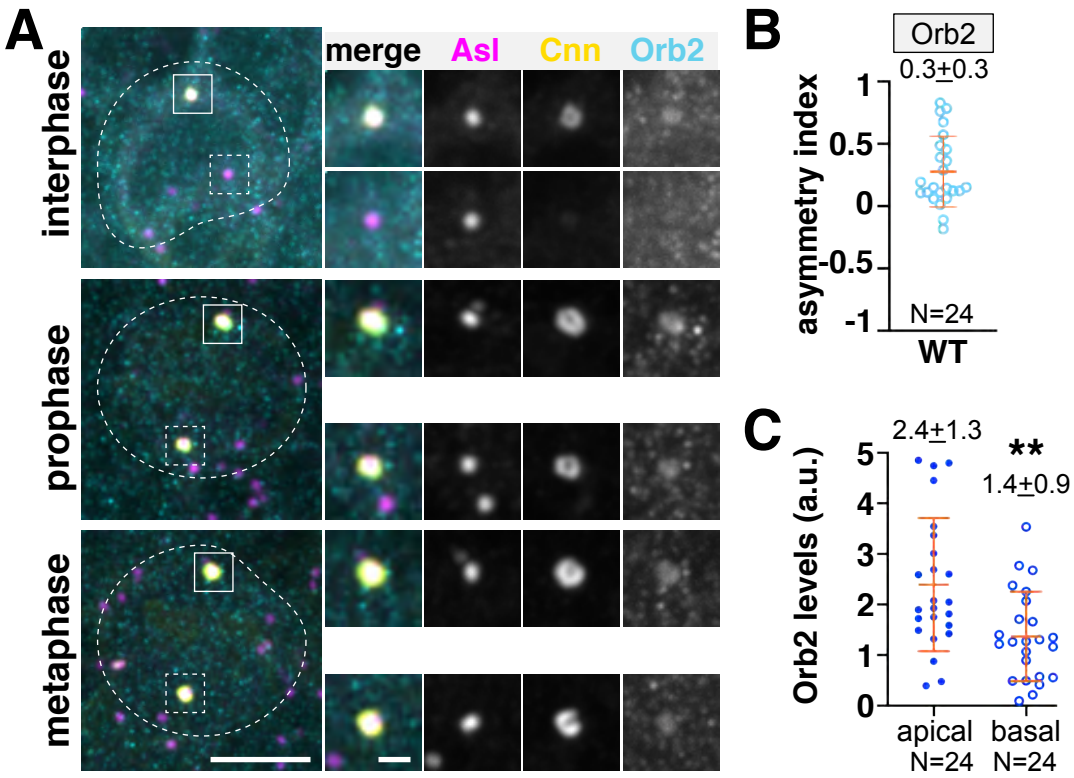

Robinson et al.

Figure 4. Orb2 localizes to active centrosomes

bioRxiv preprint doi: https://doi.org/10.1101/2021.11.23.469707; this version posted November 23, 2021. The copyright holder for this preprint (which was not certified by peer review) is the author/funder, who has granted bioRxiv a license to display the preprint in perpetuity. It is made available under aCC-BY-NC 4.0 International license.

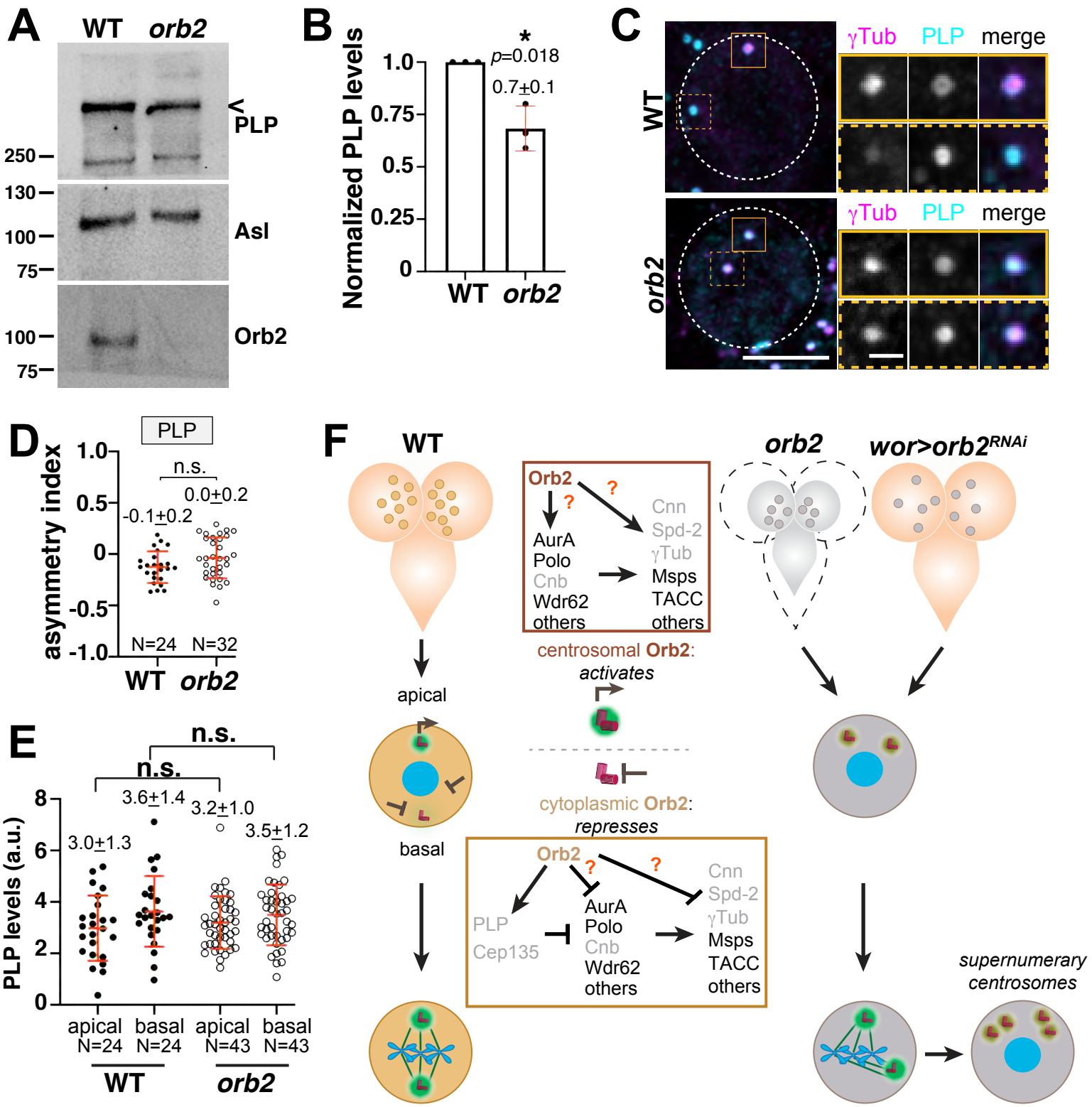

Robinson et al.
Figure 5. Orb2 regulates PLP protein levels

bioRxiv preprint doi: https://doi.org/10.1101/2021.11.23.469707; this version posted November 23, 2021. The copyright holder for this preprint (which was not certified by peer review) is the author/funder, who has granted bioRxiv a license to display the preprint in perpetuity. It is made available under aCC-BY-NC 4.0 International license.

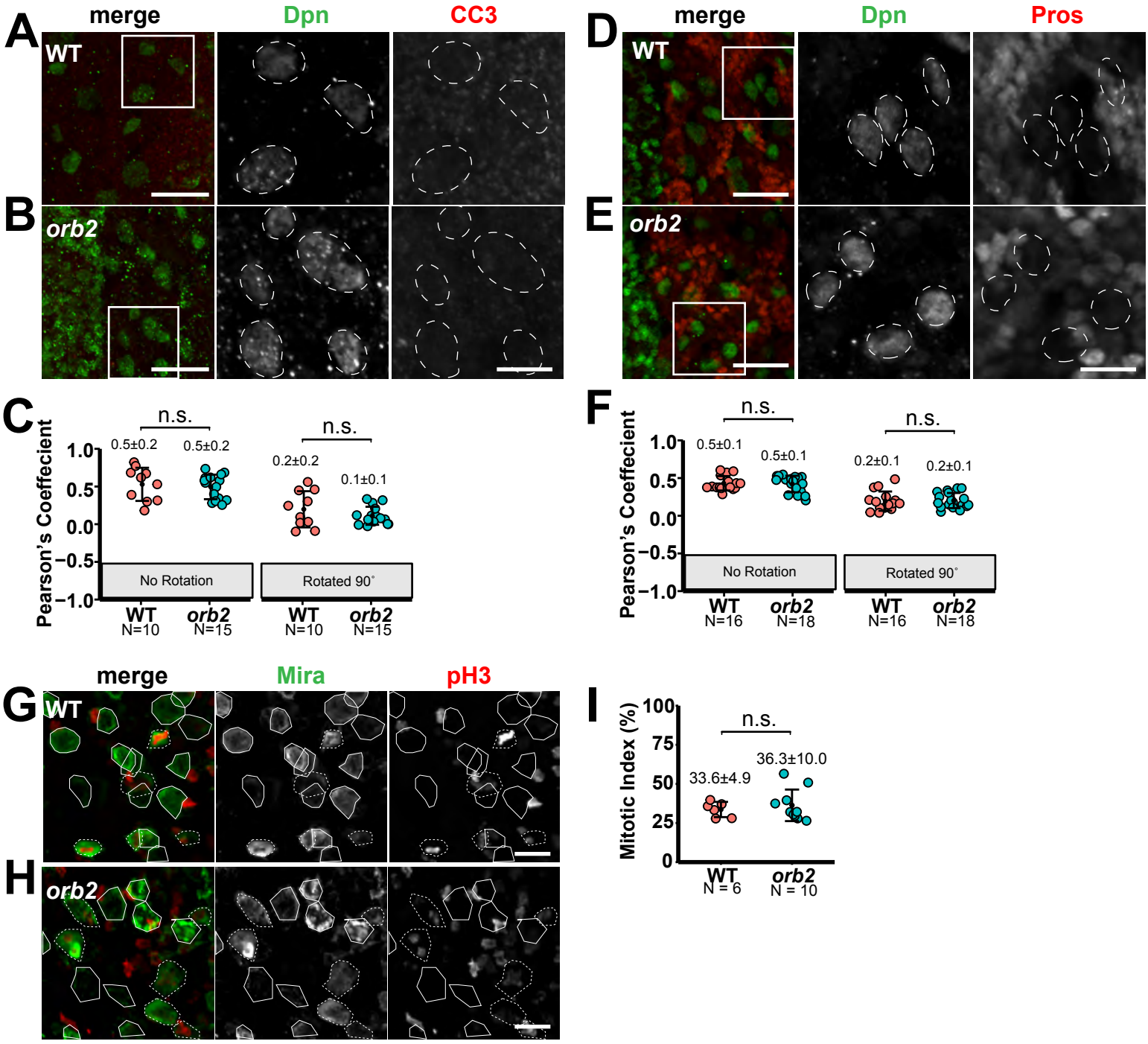

Robinson et al.
Figure S1. NSC differentiation and survival in WT vs. *orb2* mutants

bioRxiv preprint doi: https://doi.org/10.1101/2021.11.23.469707; this version posted November 23, 2021. The copyright holder for this preprint (which was not certified by peer review) is the author/funder, who has granted bioRxiv a license to display the preprint in perpetuity. It is made available under aCC-BY-NC 4.0 International license.

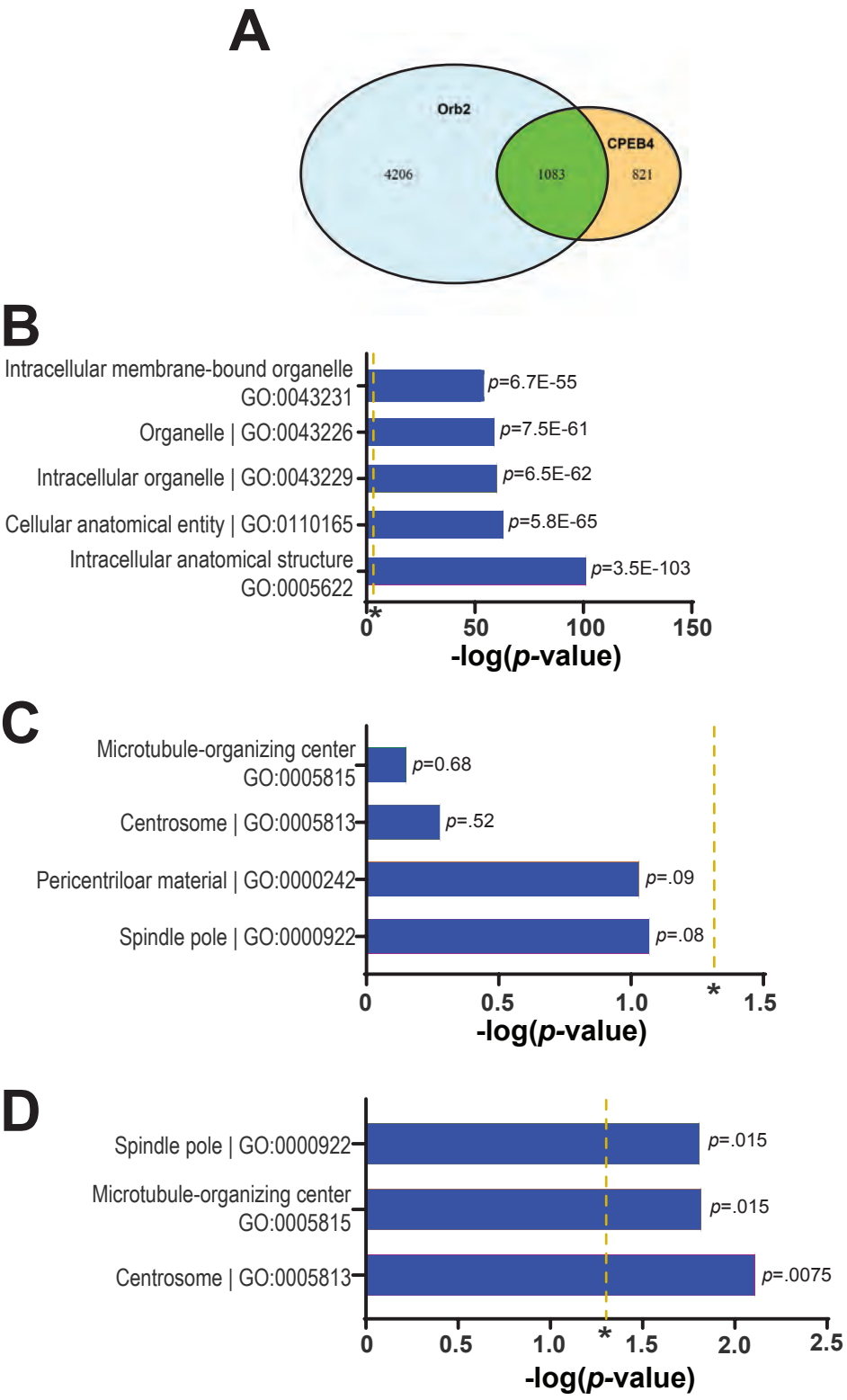

Robinson et al.
Figure S2. Ontological analysis of Orb2 and human CPEB4